Stability Analysis of Cascaded System With Multiple DC Buses Based on Positive-Mode Damping Criterion

Yuhang Yang, *Student Member, IEEE*, Yanfeng Chen, *Member, IEEE*, Bo Zhang, *Fellow, IEEE*, Dongyuan Qiu, *Senior Member, IEEE*, and Fan Xie, *Member, IEEE*

***Abstract*—The coupling between various levels of buses in a cascaded system may cause instability of the entire system. The traditional Nyquist criterion is not convenient for predicting the oscillation frequency and some extra steps might be needed for the possible right half plane poles. Therefore, new stability criteria are desired to analyze the stability of this type of hybrid system. In this article, taking a cascaded system containing an ac–dc converter and multiple dc–dc converters as an example, the small signal impedance model of the system is first established and analyzed in detail according to the mutual coupling principle between different converters. Second, based on positive-mode damping criterion, a simple stability assessment method for cascaded systems is proposed. By analyzing the real and imaginary parts of the eigenvalues of the closed-loop transfer function matrix, the stability state and the oscillation frequency of the system can be obtained. Finally, the relationship between the coupling degree of each converter and the oscillation of bus voltage is explored and a case analysis is given. The proposed model and stability analysis results are verified both by simulations and semiphysical hardware experiments.**

***Index Terms*—Cascaded system, multiple dc buses, positive-mode damping (PMD), stability analysis.**

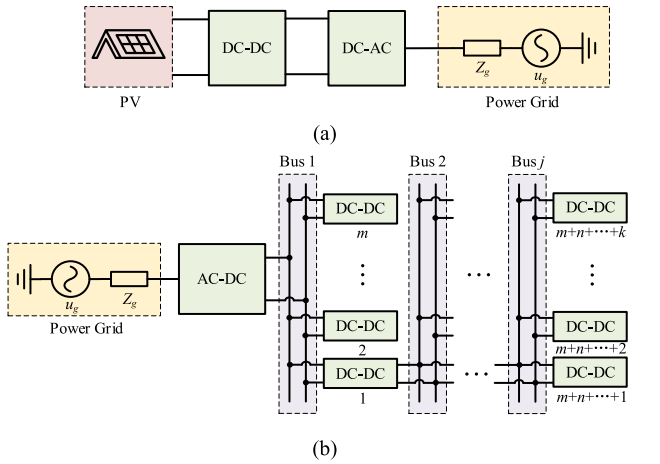

Fig. 1. (a) Photovoltaic power generation system and (b) distribution system with multiple DC buses.

I. Introduction

With the continuous development of renewable energy sources, the proportion and the importance of power electronic equipment in the power system is gradually increasing [1], [2], [3]. In order to transfer energy better, the cascaded structure has been widely used [4]. For instance, in the field of photovoltaic generation system, as shown in Fig. 1(a), a dc–dc converter is placed in front of the inverter to boost the voltage, so as to reduce the requirements of the output voltage of the photovoltaic panel [5]. On the distribution side, due to the existence of various dc equipment with different supply voltages, it is often necessary to use an ac–dc converter to get dc power first, and then adopt a cascaded structure that contains multiple dc buses to supply power for equipment in different situations [6], as shown in Fig. 1(b).

When one bus of a cascaded system becomes unstable, the oscillation may be transmitted to other devices, thus causing instability of the whole system. For the small signal stability of a system, there are currently two main methods, i.e., the state-space averaging (SSA) method [7], [8], [9] and the impedance analysis method [10], [11]. The SSA method can provide a clear understanding of the various states within the system, but this method requires prior knowledge of the system parameters, including specific details of the main circuit and controller, which is often difficult to be obtained in practice [12]. In the meanwhile, as the order of the system gradually increases, it becomes hard to establish the state-space model of the system [13]. On the contrary, the impedance analysis method equates the system to an impedance series—a voltage source (or an admittance parallel—a current source) [10], and its mathematical model can be established through specific circuit modeling or directly measuring the electrical quantities of the corresponding ports without knowing the system parameters. Compared to the SSA, the impedance analysis method can simply analyze and has been extensively studied [14].

Manuscript received 24 November 2023; revised 1 March 2024; accepted 27 April 2024. Date of publication 8 May 2024; date of current version 20 June 2024. This work was supported by the National Natural Science Foundation of China under Grant U2166601. Recommended for publication by Associate Editor M. Liserre. *(Corresponding author: Yanfeng Chen.)*

The authors are with the School of Electric Power, South China University of Technology, Guangzhou 510640, China (e-mail: epyuhangyang@mail.scut.edu.cn; eeyfchen@scut.edu.cn; epbzhang@scut.edu.cn; epdyqiu@scut.edu.cn; epfxie@scut.edu.cn).

Color versions of one or more figures in this article are available at https://doi.org/10.1109/TPEL.2024.3398035.

Digital Object Identifier 10.1109/TPEL.2024.3398035

In [14], [15], and [16], the interaction between single converter and the power grid was discussed. The authors in [17], [18], [19], and [20] extended the object to multiconverters, but mainly focused on studying the stability with parallel structure. Even if the system contained cascaded structure, these references generally tended to view it as a whole, i.e., the stability of the output ports. As for the cascaded system with multi-dc buses, in order to ensure that there are no right half plane (RHP) poles, and thus not spend more time to calculate the number of RHP poles, a step-by-step analysis method was proposed in [21]. First, the stability of each converter in the last stage is guaranteed so that the input impedances of these converters do not contain RHP poles. Then, these input impedances are taken as the equivalent load of the upper stage and the stability is analyzed by Nyquist criterion (NC) until traversing the whole system. The stability assessment method is somewhat complex and time-consuming. In addition, this method ignored the influence of the upper stage when studying the lower stage. In [22], an unterminated two-port model was proposed and the stability of a cascaded system with dc–dc converters was studied with passivity criterion. However, on the one hand, the passivity criterion may be conservative and cannot provide the instability frequency of the system. On the other hand, its main research objects were dc–dc converter and ac–dc converter as loads in off-grid condition, and there was a lack of attention to the interaction between ac–dc converter and dc–dc converter in weak power grids.

A stability criterion called positive-mode damping (PMD) criterion was proposed in [23], which is based on the closed-loop transfer function. By analyzing the real part and imaginary part characteristics of the eigenvalues of the system matrix, the stability of the system can be judged, thereby avoiding the RHP poles. Besides, the instability frequency of the system can be predicted. The scenario of multiparalleled grid-connected converters is studied in [23], without involving cascaded systems. This article attempts to fill this gap, applying this method to the stability analysis of a more complex cascaded hybrid system with multiple dc buses, which consists of an ac–dc converter and several different types of dc–dc converters, such as buck and boost converters. A detailed derivation of the model required for studying the stability of the cascaded system is provided, which takes into account the effects of each level of the buses. Then, based on the obtained model and combined with PMD criterion, a cascaded system stability assessment method is proposed and the stability of the system can be explored.

Compare with the time-domain-based eigenvalue criterion of coefficient matrix of state-space equations and s-domain-based generalized Nyquist criterion (GNC), there are some characteristics of the proposed method as follows.

1) Few steps: Different from GNC, the method does not need to consider the RHP poles. Besides, when the constructures or parameters of the system are not variable, in order to determine the stability of the system through the state equation, it is necessary to first obtain the closed-loop transfer function, then convert it into a state-space expression, and finally obtain the eigenvalues of the coefficient matrix, which is complex and time-consuming. The method used in this article does not require the derivation and can directly assess stability through the eigenvalues of transfer function.
2) Wide application range: For the closed-loop transfer function, it can be obtained not only by system data, but also by system measurement, making it suitable for these scenarios in which the systems are black-boxes due to trade secret or user privacy.
3) By drawing the variations of the eigenvalues of the closed-loop transfer function, it will be easy and intuitive to judge the system stability and the oscillation mode [23].

The main contributions of this article are summarized as follows.

1) A detailed small signal model of the cascaded system with multiple dc buses is derived. On this basis, the article discusses how each stage of the system affects each other and reveals that the effects can be reflected in changing the equivalent input impedance or output impedance of the subsystem. Besides, when the number of cascades increases, a gradual stability assessment strategy is proposed, decreasing the complexity of model and the computer calculation time.
2) The PMD criterion is used in ac/dc hybrid system and it expands the application range of the criterion.
3) The relationship between the coupling degree of each converter and the oscillation of bus voltage is investigated and the function of the filter capacitor C_{dc} between the ac–dc converter and dc–dc converter is discussed. The result shows that increasing the coupling between the converters appropriately may reduce the oscillation of the overall system buses. It implies that the coupling has also the potential to play a positive impact on the stability of the system and provides a new idea for the future controller design.

The rest of this article is organized as follows. Section II studies the cascaded system with multiple dc buses and the impedance model of each part is presented. The principle of PMD criterion is introduced in Section III. In Section IV, how to establish a comprehensive mathematical model for a cascaded system that considers the impact of each level of converter on the bus is discussed in detail, and a specific assessment strategy is given. Stability analyses based on simulation and experiment are presented in Sections V and VI, respectively. Finally, Section VII concludes this article.

II. Model of Cascaded System With Multiple DC Buses

The structure of the studied cascaded system with multiple dc buses is shown in Fig. 2. The power grid is connected to a three-phase ac–dc converter and its energy is transferred to the dc side. Several dc–dc converters are connected through dc buses. For simplicity, a two-stage cascade system is designed on the premise of without loss of generality. Meanwhile, different from the system in [21], in addition to buck, a boost converter is introduced to the cascaded system, which can better reflect the general applicability of the proposed method.

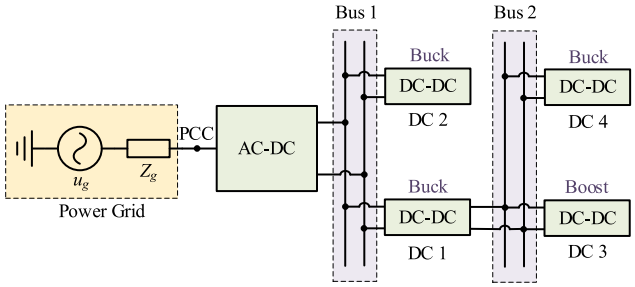

Fig. 2. Cascaded system with two DC buses.

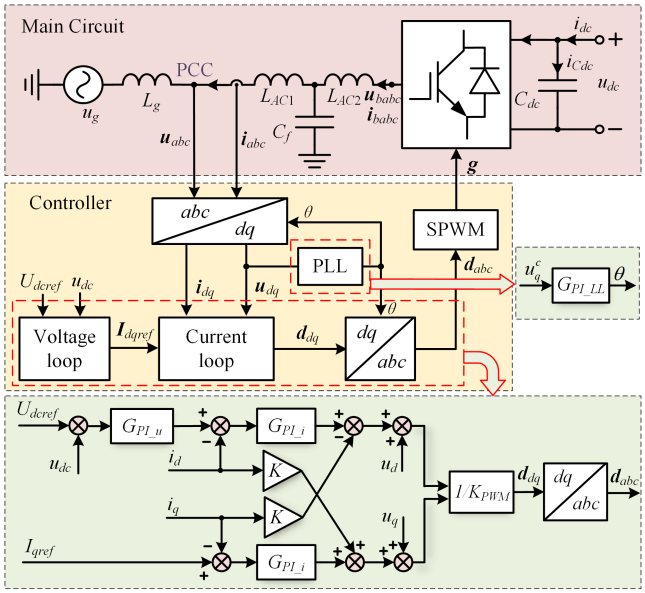

Fig. 3. System diagram of the AC–DC converter.

A. Model of the Three-Phase AC–DC Converter

The three-phase ac–dc converter is shown in Fig. 3 and a universal single-line circuit diagram is used to represent the three-phase circuit for simplicity [14], [25]. The main circuit adopts three-phase full-bridge topology and *LCL* filter, and the control part is a voltage and current dual closed-loop control in the *dq* coordinate system. The Bus 1 voltage is compared to a reference and the difference is then used by a PI controller to generate the reference value of the current inner loop. The current loop includes cross-decoupling and point of common coupling (PCC) voltage feedforward. Finally, the duty in the *dq* coordinate system is converted back to its counterpart value in the *abc* coordinate system through inverse Park transform and the driving signal is generated through a sinusoidal pulse width modulation (SPWM) module to adjust the output of the converter.

The variables with subscript "*abc*" and "*dq*" are the vectors under the *abc* three-phase coordinate and *dq* coordinate system, respectively. For example, $\boldsymbol{u}_{abc} = [u_a, u_b, u_c]^T$ and $\boldsymbol{u}_{dq} = [u_d, u_q]^T$, where u_a, u_b, and u_c are the three-phase PCC voltages, and u_d and u_q are the *d*-axis and *q*-axis components of the PCC voltage, respectively.

1) Main Circuit: According to the instantaneous power balance and the Park transform, there are

$$\begin{cases} u_{\rm dc}\left(i_{\rm dc} - i_{C\rm dc}\right) = \frac{3}{2}\begin{bmatrix} u_{bd} & u_{bq} \end{bmatrix}\begin{bmatrix} i_{bd} \\ i_{bq} \end{bmatrix} \\ i_{C\rm dc} = C_{\rm dc}\frac{du_{\rm dc}}{dt} \end{cases} \tag{1}$$

where u_{bd}, u_{bq}, i_{bd}, and i_{bq} are the *d*-axis and *q*-axis components of the bridge leg side voltage and current, respectively.

Injecting small signal disturbances into each variable in (1), i.e.,

$$\begin{cases} u_{\rm dc} = U_{\rm dc} + \Delta u_{\rm dc},\ i_{\rm dc} = I_{\rm dc} + \Delta i_{\rm dc} \\ u_{bd} = U_{bd} + \Delta u_{bd} \approx U_d + \Delta u_{bd} \\ u_{bq} = U_{bq} + \Delta u_{bq} \approx U_q + \Delta u_{bq} \\ i_{bd} = I_{bd} + \Delta i_{bd} \approx I_d + \Delta i_{bd} \\ i_{bq} = I_{bq} + \Delta i_{bq} \approx I_q + \Delta i_{bq}. \end{cases} \tag{2}$$

Lowercase letters represent the instantaneous values and capital letters stand for the steady-state values. Besides, the symbol "Δ" before a physical quantity represents the small signal variation.

Linearization is then performed to obtain the steady-state points and the small signal expressions of the main circuit

$$U_{\rm dc} I_{\rm dc} = \frac{3}{2}\begin{bmatrix} U_{bd} & U_{bq} \end{bmatrix}\begin{bmatrix} I_d \\ I_q \end{bmatrix} \tag{3}$$

$$\begin{aligned} &U_{\rm dc}\Delta i_{\rm dc} + I_{\rm dc}\Delta u_{\rm dc} - C_{\rm dc}U_{\rm dc}\frac{d\Delta u_{\rm dc}}{dt} \\ &= \frac{3}{2}\left(\begin{bmatrix} U_d & U_q \end{bmatrix}\begin{bmatrix} \Delta i_{bd} \\ \Delta i_{bq} \end{bmatrix} + \begin{bmatrix} I_d & I_q \end{bmatrix}\begin{bmatrix} \Delta u_{bd} \\ \Delta u_{bq} \end{bmatrix}\right). \end{aligned} \tag{4}$$

Similarly, the small signal expression of *LCL* filter can be obtained and there is

$$\begin{cases} \Delta \boldsymbol{i}_{dq} = \boldsymbol{G}_1\Delta \boldsymbol{u}_{dq} + \boldsymbol{G}_2\Delta \boldsymbol{u}_{bdq} \\ \Delta \boldsymbol{i}_{bdq} = \boldsymbol{G}_3\Delta \boldsymbol{i}_{dq} + \boldsymbol{G}_4\Delta \boldsymbol{u}_{dq} \end{cases} \tag{5}$$

where $\boldsymbol{u}_{bdq}$ and $\boldsymbol{i}_{bdq}$ are the bridge leg side voltage vector and current vector ($\boldsymbol{u}_{bdq} = [u_{bd}, u_{bq}]^T$, $\boldsymbol{i}_{bdq} = [i_{bd}, i_{bq}]^T$)

$$\begin{cases} \boldsymbol{G}_1 = -(\boldsymbol{Z}_{LAC1} + \boldsymbol{Z}_{LAC2} + \boldsymbol{Z}_{LAC1}\boldsymbol{Y}_{Cf}\boldsymbol{Z}_{LAC2})^{-1}(\boldsymbol{E} + \boldsymbol{Z}_{LAC1}\boldsymbol{Y}_{Cf}) \\ \boldsymbol{G}_2 = (\boldsymbol{Z}_{LAC1} + \boldsymbol{Z}_{LAC2} + \boldsymbol{Z}_{LAC1}\boldsymbol{Y}_{Cf}\boldsymbol{Z}_{LAC2})^{-1} \\ \boldsymbol{G}_3 = \boldsymbol{E} + \boldsymbol{Y}_{Cf}\boldsymbol{Z}_{LAC2} \\ \boldsymbol{G}_4 = \boldsymbol{Y}_{Cf}. \end{cases} \tag{6}$$

The specific expressions of $\boldsymbol{Z}_{LAC1}$, $\boldsymbol{Z}_{LAC2}$, and $\boldsymbol{Y}_{Cf}$ are given in the Appendix and $\boldsymbol{E}$ is a 2×2 identity matrix.

Based on (5) and (6), applying Laplace transform to (4) yields

$$\Delta \boldsymbol{u}_{\rm dc} = \boldsymbol{Y}_{oac}^{-1}\Delta \boldsymbol{i}_{\rm dc} + \boldsymbol{G}_{iu\rm dc}\Delta \boldsymbol{i}_{dq} + \boldsymbol{G}_{uu\rm dc}\Delta \boldsymbol{u}_{dq} \tag{7}$$

where $Y_{oac} = sC_{\rm dc}$ and the detailed expressions of $\boldsymbol{G}_{iu\rm dc}$ and $\boldsymbol{G}_{uu\rm dc}$ are also given in the Appendix.

2) Phase-Locked Loop (PLL): Considering the dynamic characteristic of phase-locked loop (PLL), there is a phase difference between the main circuit and the control system, which can be expressed as $\Delta\theta = \theta^c - \theta^s$ (superscripts "*s*" and "*c*" represent the variables of system and controller, respectively).

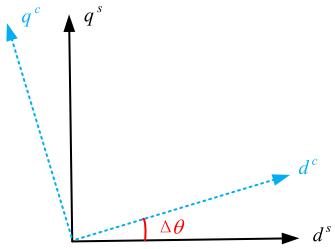

Fig. 4. Difference phase between two dq coordinate.

From Fig. 4, the relationship of variables between two coordinate systems can be written as follows:

$$\begin{bmatrix} x_d^c \\ x_q^c \end{bmatrix} = \begin{bmatrix} \cos\Delta\theta & \sin\Delta\theta \\ -\sin\Delta\theta & \cos\Delta\theta \end{bmatrix} \begin{bmatrix} x_d^s \\ x_q^s \end{bmatrix} \approx \begin{bmatrix} 1 & \Delta\theta \\ -\Delta\theta & 1 \end{bmatrix} \begin{bmatrix} x_d^s \\ x_q^s \end{bmatrix} \tag{8}$$

where "x" can be voltage u, current i, or duty ratio d, and so on, and it can be further derived from (8) that

$$\begin{bmatrix} \Delta x_d^c \\ \Delta x_q^c \end{bmatrix} \approx \begin{bmatrix} \Delta x_d^s + \Delta\theta X_q^s \\ \Delta x_q^s - \Delta\theta X_d^s \end{bmatrix} = \begin{bmatrix} \Delta x_d^s \\ \Delta x_q^s \end{bmatrix} + \Delta\theta \begin{bmatrix} X_q^s \\ -X_d^s \end{bmatrix} \tag{9}$$

where $\Delta q = G_{\text{PI\_PLL}}\Delta u_q^c$ and $G_{\text{PI·PLL}}$ is the PI controller of PLL. So (9) can be rewritten in detail as

$$\begin{cases} \Delta \boldsymbol{u}_{dq}^c = \begin{bmatrix} 1 & G_{\text{PLL}}U_q^s \\ 0 & 1 - G_{\text{PLL}}U_d^s \end{bmatrix} \Delta \boldsymbol{u}_{dq}^c \triangleq \boldsymbol{G}_{\text{PLL}}^u \Delta \boldsymbol{u}_{dq}^s \\ \Delta \boldsymbol{i}_{dq}^c = \Delta \boldsymbol{i}_{dq}^s + \begin{bmatrix} 0 & G_{\text{PLL}}I_q^s \\ 0 & -G_{\text{PLL}}I_d^s \end{bmatrix} \Delta \boldsymbol{u}_{dq}^s \triangleq \Delta \boldsymbol{i}_{dq}^s + \boldsymbol{G}_{\text{PLL}}^i \Delta \boldsymbol{u}_{dq}^s \\ \Delta \boldsymbol{d}_{dq}^s = \Delta \boldsymbol{d}_{dq}^c + \begin{bmatrix} 0 & -G_{\text{PLL}}D_q^c \\ 0 & G_{\text{PLL}}D_d^c \end{bmatrix} \Delta \boldsymbol{u}_{dq}^s \triangleq \Delta \boldsymbol{d}_{dq}^c + \boldsymbol{G}_{\text{PLL}}^d \Delta \boldsymbol{u}_{dq}^s \end{cases} \tag{10}$$

in which $G_{\text{PLL}} = G_{\text{PI·PLL}}/(s+U_d G_{\text{PI·PLL}})$.

3) Controller: According to Fig. 3, there is

$$\begin{cases} \Delta \boldsymbol{d}_{dq}^c = \frac{1}{K_{\text{PWM}}}[\Delta \boldsymbol{u}_{dq}^c + (\boldsymbol{G}_i - \boldsymbol{G}_{i\_L})(\Delta \boldsymbol{i}_{dq\text{ref}}^c - \Delta \boldsymbol{i}_{dq}^c)] \\ \Delta \boldsymbol{i}_{dq\text{ref}}^c = \boldsymbol{G}_u(\Delta \boldsymbol{u}_{\text{dcref}} - \Delta \boldsymbol{u}_{\text{dc}}) \end{cases} \tag{11}$$

where

$$\Delta \boldsymbol{i}_{dq\text{ref}}^c = \begin{bmatrix} \Delta i_{d\text{ref}}^c \\ \Delta i_{q\text{ref}}^c \end{bmatrix},\ \Delta \boldsymbol{u}_{\text{dcref}} = \begin{bmatrix} \Delta u_{\text{dcref}} \\ 0 \end{bmatrix},\ \Delta \boldsymbol{u}_{\text{dc}} = \begin{bmatrix} \Delta u_{\text{dc}} \\ 0 \end{bmatrix} \tag{12}$$

$$\begin{cases} \boldsymbol{G}_{i\_L} = \begin{bmatrix} 0 & \omega_0(L_{AC1} + L_{AC2}) \\ -\omega_0(L_{AC1} + L_{AC2}) & 0 \end{bmatrix} \\ \boldsymbol{G}_i = \begin{bmatrix} G_{\text{PI\_}i} & 0 \\ 0 & G_{\text{PI\_}i} \end{bmatrix},\ \boldsymbol{G}_u = \begin{bmatrix} G_{\text{PI\_}u} & 0 \\ 0 & G_{\text{PI\_}u} \end{bmatrix}. \end{cases} \tag{13}$$

$G_{\text{PI·}i}$ and $G_{\text{PI·}u}$ are the PI controllers of current loop and voltage loop, respectively.

Based on above analysis, the ac–dc converter's small signal model can be obtained and it is shown in Fig. 5.

According to Fig. 5, the model of the ac–dc converter in admittance matrix form can be written as follows:

$$\begin{bmatrix} \Delta \boldsymbol{i}_{dq} \\ \Delta \boldsymbol{i}_{\text{dc}} \end{bmatrix} = \begin{bmatrix} -\boldsymbol{Y}_{iac} & \boldsymbol{Y}_{da} & \boldsymbol{Y}_{rda} \\ \boldsymbol{Y}_{ad} & \boldsymbol{Y}_{oac} & \boldsymbol{Y}_r \end{bmatrix} \begin{bmatrix} \Delta \boldsymbol{u}_{dq} \\ \Delta \boldsymbol{u}_{\text{dc}} \\ \Delta \boldsymbol{u}_{\text{dcref}} \end{bmatrix} \tag{14}$$

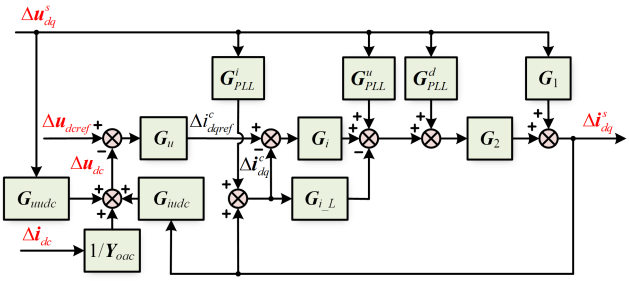

Fig. 5. Small signal model of three-phase AC–DC converter.

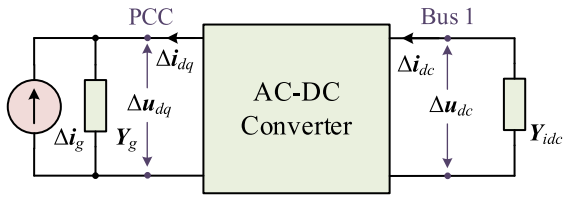

Fig. 6. Port model of three-phase AC–DC converter considering power grid and DC side circuit.

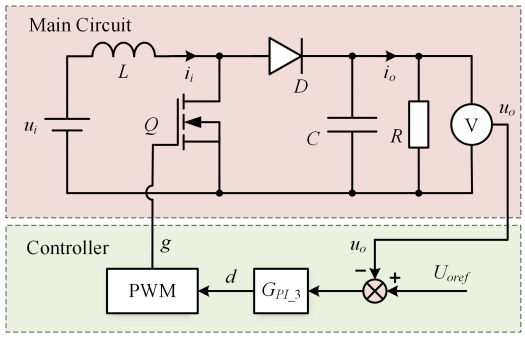

Fig. 7. System diagram of DC 3 (boost converter).

where all admittance matrixes are 2×2 and they are transfer functions between different variables. For example, $\boldsymbol{Y}_{oac}$ is the transfer function from $\Delta \boldsymbol{u}_{\text{dc}}$ to $\Delta \boldsymbol{i}_{\text{dc}}$ and there is

$$\begin{aligned} \Delta \boldsymbol{i}_{\text{dc}} &= \boldsymbol{Y}_{oac}\Delta \boldsymbol{u}_{\text{dc}}|_{\Delta \boldsymbol{u}_{dq}=0,\ \Delta \boldsymbol{u}_{\text{dcref}}=0} \\ \Rightarrow \begin{bmatrix} \Delta i_{\text{dc}} \\ 0 \end{bmatrix} &= \begin{bmatrix} sC_{\text{dc}} & 0 \\ 0 & 0 \end{bmatrix} \begin{bmatrix} \Delta u_{\text{dc}} \\ 0 \end{bmatrix} \Big|_{\Delta \boldsymbol{u}_{dq}=0,\ \Delta \boldsymbol{u}_{\text{dcref}}=0}. \end{aligned} \tag{15}$$

If Norton theorem is applied to the power grid and the dc circuit equivalent input admittance $\boldsymbol{Y}_{\text{idc}}$ is considered, and the Δu_{dcref} is ignored, then the port model of the ac–dc converter that includes the power grid and dc circuits can be obtained, as shown in Fig. 6, in which Y_g is the gird admittance and the voltage and current relationship of the port are determined by (14).

B. Model of the DC–DC Converter

Fig. 7 gives the control diagram of dc 3 (boost converter). All dc–dc converters in the system adopt the voltage-mode PWM controller with the PI-based regulation. It is worth noting

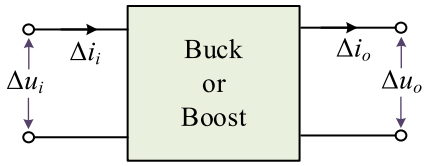

Fig. 8. Two-port model of DC–DC converter.

that the power of dc–dc converters is decided by the specific loads and the voltage of dc buses, where the power transmitted via dc 1 is equivalent to the sum of dc 3 and dc 4, namely $P_1 = P_3 + P_4$.

Based on Fig. 7 and the prior knowledge of boost, there are

$$\begin{bmatrix} \frac{di_i}{dt} \\ \frac{du_o}{dt} \end{bmatrix} = \begin{bmatrix} 0 & -\frac{1-d}{L} \\ \frac{1-d}{C} & -\frac{1}{RC} \end{bmatrix} \begin{bmatrix} i_i \\ u_o \end{bmatrix} + \begin{bmatrix} \frac{1}{L} \\ 0 \end{bmatrix} u_i. \tag{16}$$

Making (16) equal to 0 gives the values of state variables of the boost converter in steady state, i.e., $U_o = [1/(1-D)]U_i$ and $I_i = U_o/[R(1-D)]$. Similar to the ac–dc converter, the small signal disturbances and linearization are used to get the steady-state model and small-signal model

$$\begin{bmatrix} \Delta i_i \\ \Delta i_o \end{bmatrix} = \begin{bmatrix} Y_i & Y_{oi} & G_{dii} \\ Y_{io} & -Y_o & G_{dio} \end{bmatrix} \begin{bmatrix} \Delta u_i \\ \Delta u_o \\ \Delta d \end{bmatrix}. \tag{17}$$

For the matrix elements in (17), they are the transfer functions between different signals. Taking Y_i as an example, it is the transfer function from Δu_i to Δi_i and there is $Y_i = (\Delta i_i/\Delta u_i)|_{\Delta u_o = 0, \Delta d = 0}$. The detailed expressions are given in the Appendix.

When the feedback control is adopted, the Δd can be changed as follows if the single voltage loop control is used

$$\Delta d = G_c G_{\text{del}} [\Delta u_{\text{oref}} - \Delta u_o] \tag{18}$$

where G_c is the PI controller and $G_c = G_{\text{PI·3}}$ here. G_{del} represents the delay and it can be written approximately [21] as

$$G_{\text{del}} = \frac{T_d^2 s^2 - 6T_d s + 12}{T_d^2 s^2 + 6T_d s + 12} \tag{19}$$

where T_d is the delay time.

Ignoring Δu_{oref} and eliminating Δd by substituting (18) into (17), then the main circuit of either boost converter or buck converter can be represented by a two-port network, as shown in Fig. 8, and (17) turns into

$$\begin{bmatrix} \Delta i_i \\ \Delta i_o \end{bmatrix} = \begin{bmatrix} Y_i & Y_{oi} - G_{dii} G_c G_{\text{del}} \\ Y_{io} & -Y_o - G_{dio} G_c G_{\text{del}} \end{bmatrix} \begin{bmatrix} \Delta u_i \\ \Delta u_o \end{bmatrix}. \tag{20}$$

When the stability of dc buses is analyzed, the output admittance of ac–dc converter also needs to be considered, and the details will be further investigated in Section IV.

III. Positive-Mode Damping Criterion Based on Closed-Loop Transfer Function

For a multi-inputs multioutputs system, its small signal s-domain model is

$$\Delta \boldsymbol{y}(s) = \boldsymbol{\Phi}(s) \Delta \boldsymbol{u}(s) \tag{21}$$

where $\Delta \boldsymbol{y}(s)$ and $\Delta \boldsymbol{u}(s)$ are output and input variable vectors, respectively, $\Delta \boldsymbol{y}(s) = [\ \Delta y_1,\ \Delta y_2,\ \ldots]^T$ and $\Delta \boldsymbol{u}(\mathrm{s}) = [\Delta u_1,\ \Delta u_2,\ \ldots]^T$.

In general, eigenvalue is a concept that suits for the complex-domain. However, as introduced in [26], the meaning of eigenvalues can be extended to the s-domain and the eigenvalues of $\Phi(\mathrm{s})$ can be defined as the solutions of the equation as follows:

$$\det[\lambda(s)\boldsymbol{I} - \boldsymbol{\Phi}(s)] = \boldsymbol{0}. \tag{22}$$

In most cases, as discussed in [26], the poles of the eigenvalues of the closed-loop transfer function matrix $\Phi(s)$ are the poles of $\Phi(s)$, so $\lambda(s)$ can be used to assess the stability of the system.

Assuming that one of the eigenvalues $\lambda_i(s)$ is expressed as

$$\lambda_i(s) = \frac{\prod_{k=1}^{u} [(s - z_k)(s - z_k^*)] \prod_{g=1}^{t} (s - z_g)}{s^h \prod_{l=1}^{v} [(s - p_l)(s - p_l^*)] \prod_{q=1}^{n} (s - p_q)} \tag{23}$$

where h is the number of integral links, z_k and z_k^* are the conjugate zeros, and z_g is the real zero. Similarly, p_l and p_l^* are the conjugate poles and p_q is the real pole. Assuming p_m and p_m^* are one of a pair of conjugates and they can be written as $(\sigma_m \pm j\omega_m)$. Substituting s with $j\omega$, then (23) can be further expressed as

$$\begin{aligned} \lambda_i(j\omega) &= \frac{\prod_{k=1}^{u} [(j\omega - z_k)(j\omega - z_k^*)] \prod_{g=1}^{t} (j\omega - z_g)}{(j\omega)^h \prod_{l=1,\, l \neq m}^{v} [(j\omega - p_l)(j\omega - p_l^*)] \prod_{q=1}^{n} (j\omega - p_q)} \\ &\quad \times \frac{1}{(j\omega - p_m)(j\omega - p_m^*)} \\ &\triangleq \frac{G_i(j\omega)}{(j\omega - p_m)(j\omega - p_m^*)} = \frac{G_i(j\omega)}{(\omega_m^2 - \omega^2 + \sigma_m^2) - j2\sigma_m\omega} \end{aligned} \tag{24}$$

where $G_i(j\omega)$ is the rest part of $\lambda_i(j\omega)$ except for the pair of conjugate poles and it has $G_i(j\omega) = G_{i,r}(j\omega) + jG_{i,i}(j\omega)$.

So the real part $\lambda_{i,r}(j\omega)$ and the imaginary part $\lambda_{i,i}(j\omega)$ of (24) can be, respectively, derived as follows:

$$\begin{cases} \lambda_{i,r}(j\omega) = \frac{(\omega_m^2 - \omega^2 + \sigma_m^2) G_{i,r}(j\omega) - 2\sigma_m \omega G_{i,i}(j\omega)}{(\omega_m^2 - \omega^2 + \sigma_m^2)^2 + (2\sigma_m\omega)^2} \\ \lambda_{i,i}(j\omega) = \frac{(\omega_m^2 - \omega^2 + \sigma_m^2) G_{i,i}(j\omega) + 2\sigma_m \omega G_{i,r}(j\omega)}{(\omega_m^2 - \omega^2 + \sigma_m^2)^2 + (2\sigma_m\omega)^2}. \end{cases} \tag{25}$$

By solving $\lambda_{i,i}(j\omega) = 0$, the zero-crossing frequency ω_r of $\lambda_{i,i}(j\omega)$ can be obtained, namely

$$\omega_r = \frac{2\sigma_m G_{i,r} \pm \sqrt{(2\sigma_m G_{i,r})^2 + 4(\sigma_m^2 + \omega_m^2) G_{i,i}^2}}{2G_{i,i}}. \tag{26}$$

It is well-known that a system is stable when all of its poles have negative real parts, whereas the system is unstable whenever one of the poles has a positive real part. Yet, as discussed in [23] and [24], the monotonic instability caused by large positive real part occurs less in the power system. Besides, when there is a pole with a very small absolute value of the real part, it indicates that the system is in poorly damped oscillatory mode and the system is unstable (the real part is positive) or weakly

stable (the real part is negative). When perturbed, the weakly stabilized system takes longer to return to a steady state and it is likely to become unstable due to some parameter variations or disturbances. Based on these analyses, it can be known that the poorly damped oscillatory mode is an important situation in the power system and it is the main concern in this article. In general, it is necessary to get the poles of all eigenvalues and then analyze the stability of the system according to the polarity of the real parts of the poles. However, the authors in [23] and [24] gave a new criterion to analyze whether the system is unstable by studying the real part and imaginary part of the eigenvalues themselves.

For the poorly damped oscillatory mode, that is $|\sigma_m|<<|\omega_m|$, it can be further found from (26) that $\omega_r \approx \omega_m$, which implies that the zero-crossing frequency ω_r approximately equals to the frequency ω_m of the pole p_m.

The rational fraction $G_j(j\omega)$, consisting of zeros and poles other than p_m and p_m^*, does not change much in the neighborhood of ω_m and the value of $G_j(j\omega)$ is only related to ω_m [27]. Thus, the $\lambda_{I,r}$ and the slope of $\lambda_{i,i}$ can be approximately obtained as follows:

$$\begin{cases} \lambda_{i,r}|_{\omega=\omega_r} = \frac{\sigma_m^2 G_{i,r} - 2\sigma_m\omega_r G_{i,i}}{\sigma_m^4 + (2\sigma_m\omega_r)^2} \approx \frac{-G_{i,i}}{2\sigma_m\omega_r} \\ k_{i,i}|_{\omega=\omega_r} \triangleq \left.\frac{d\lambda_{i,i}}{d\omega}\right|_{\omega=\omega_r} = \frac{-2\omega_r G_{i,i} + 2\sigma_m G_{i,r}}{\sigma_m^4 + (2\sigma_m\omega_r)^2} \approx \frac{-G_{i,i}}{2\sigma_m^2\omega_r} \end{cases} \tag{27}$$

and there implies that

$$\sigma_m = \frac{\lambda_{i,r}}{k_{i,i}}. \tag{28}$$

Equation (28) shows that σ_m can be expressed as $\lambda_{i,r}$ divided by $k_{i,i}$, i.e., the real part of λ_i is divided by the slope of imaginary of λ_i. Thus, the system is stable if it satisfies $k_{i,i} > 0$ and $\lambda_{i,r} < 0$; or $k_{i,i} < 0$ and $\lambda_{i,r} > 0$. In other words, if dividing $\lambda_{i,r}$ by $k_{i,i}$ is greater than 0, the system is unstable.

Besides, the stability criterion can be extended to stability improvement. For example, the damping of a system is calculated by $\xi_m = -\sigma_m / \sqrt{\sigma_m^2 + \omega_m^2}$ [28], in which σ_m and ω_m can be solved by (26) ($\omega_r \approx \omega_m$) and (28), respectively. Besides, Orellana et al. [24] has introduced participation factor into the PMD criterion to locate the most sensitive nodes or converters in the ac power grid, thus making targeted improvements to the system. All of these reflect the potential of the proposed method beyond stability assessment. Due to the theme of this article being the stability analysis of ac/dc system containing multiple dc buses, and limited by the length of the article, the content on using this method for stability improvement can be considered as future research article, and will not be elaborated here.

The following will analyze that how to apply the above stability criterion in the multiple dc buses cascaded system.

IV. Stability Criterion for the Cascaded System With Multiple DC Buses

For the multi-dc buses cascaded system including ac–dc converter and dc–dc converters [i.e., the model as shown in Fig. 1(b)], the stability of dc buses and PCC need to be analyzed. According to Fig. 9(a), the studied system in this article can be divided into three parts: PCC, Bus 1, and Bus 2. Each part can be seen as a parallel connection of several subsystems, as shown in Fig. 9. Siegers et al. [22] proposed a useful unterminated model of a certain level of converter, but it did not discuss that how each level of converter affects each other. So the equivalent mathematical models of the subsystems considering the interactions are given first and then the stability of each part is analyzed by using the PMD.

Taking Bus 2 as an example, the equivalent admittance model can be seen in Fig. 9(d) and it can be written as

$$\Delta u_{o1}(s) = [-Y'_{o1}(s) + Y_{i3}(s) + Y_{i4}(s)]^{-1}[\Delta i'_{o1}(s) + \Delta i_{i3}(s) + \Delta i_{i4}(s)]. \tag{29}$$

Defining the closed-loop transfer function of Bus 2 as T_2, then $T_2 = [Y'_{o1} + Y_{i3} + Y_{i4}]^{-1}$ and the stability of Bus 2 can be assessed by analyzing the real part and imaginary part of the eigenvalues of T_2 based on the stability criterion introduced in Section IV. Besides, the admittance elements in the T_2 cannot be written directly by (20) and it needs to consider the specific loads or the connections with other converters. The detailed analyses are given as follows.

A. Bus 2

Based on the above analysis, the input admittance of dc 3 and dc 4 and the output admittance of dc 1 should be concerned when studying Bus 2. It should be noted that since the front stage of dc 1 is an ac–dc converter, and dc 1 is also connected in parallel with dc 2, the influence of these two parts needs to be taken into account when deriving the output admittance of dc 1. The specific processes are as follows.

For dc 3 and dc 4, there are

$$\begin{cases} \Delta i_{o3}(s) = Y_{ld3}(s)\Delta u_{o3}(s) = \frac{1}{R_3}\Delta u_{o3}(s) \\ \Delta i_{o4}(s) = Y_{ld4}(s)\Delta u_{o4}(s) = \frac{1}{R_4}\Delta u_{o4}(s). \end{cases} \tag{30}$$

Substitute (30) into (20), and the input admittance of dc 3 and dc 4 can be obtained

$$Y'_{ik}(s) = \frac{\Delta i_{ik}(s)}{\Delta u_{ik}(s)} = Y_{ik} + \frac{(Y_{oik} - G_{diik}G_{ck}G_{\text{delk}})Y_{iok}}{Y_{ldk} + Y_{ok} + G_{diok}G_{ck}G_{\text{delk}}} \tag{31}$$

where $k = 3$ or 4, represents dc 3 or dc 4. In addition, the admittance here is marked with a superscript "′," which distinguishes it from the unterminated model in (20).

As shown in Fig. 9, for dc 1, the ac–dc converter of the front stage affects its input voltage and the dc 2 in parallel affects its input current, so there are

$$\begin{cases} \Delta u'_{i1}(s) - \Delta u_{i1}(s) = Y_{oac}^{-1}(s)\Delta i'_{i1}(s) \\ \Delta i'_{i1}(s) = \Delta i_{i2}(s) + \Delta i_{i1}(s) \\ \Delta i_{i2}(s) = Y_{i2}(s)\Delta u_{i1}(s) + G_{ir2}(s)\Delta u_{o2\text{ref}}(s) \end{cases} \tag{32}$$

where $G_{ir2}(s)$ is the transfer function of dc 2 from $\Delta u_{o2\text{ref}}(s)$ to $\Delta i_{i2}(s)$.

Due to the existence of grid admittance Y_g, $Y_{oac}(s)$ is also affected. At this time, there is

$$\Delta \boldsymbol{u}_{dq} = \boldsymbol{Y}_g(\Delta \boldsymbol{i}_{dq} + \Delta \boldsymbol{i}_g) \tag{33}$$

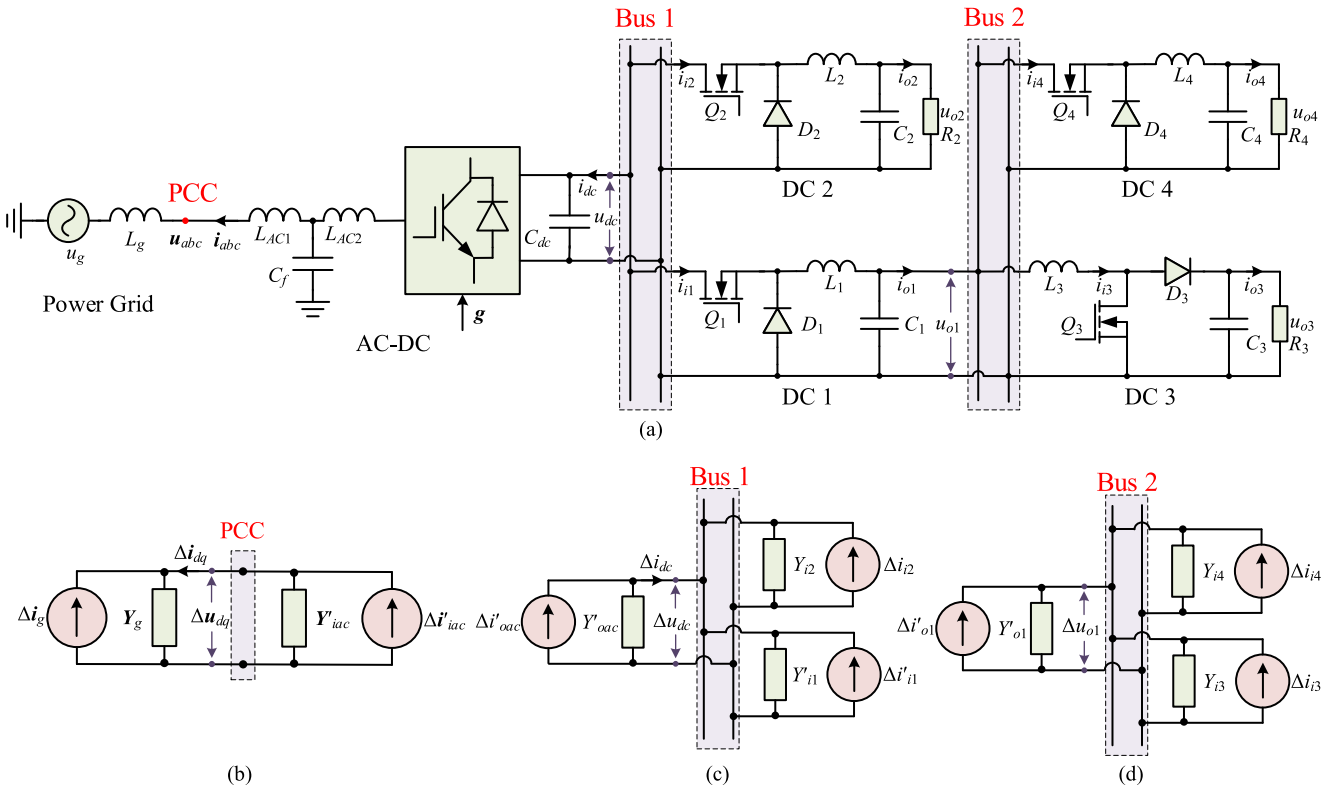

Fig. 9. (a) Detailed topology of the cascaded system. (b) Equivalent model from the view of PCC. (c) Equivalent model from the view of Bus 1. (d) Equivalent model from the view of Bus 2.

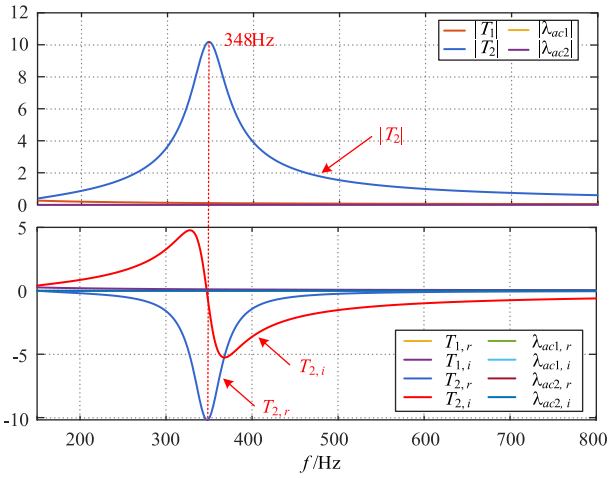

Fig. 10. Stability assessment of the cascaded system.

then substitute it to (14), so as to get the new output impedance of ac–dc converter Y'_{oac}. After that, taking $\Delta u'_{i1}$ and $\Delta i'_{i1}$ as the new input voltage and input current of dc 1, and its output admittance can be obtained using (20) and (32)

$$Y'_{o1} = Z'^{-1}_{o1} = \left.\frac{u_{o1}}{i_{o1}}\right|_{u_g=0,\ u_{o1\mathrm{ref}}=0,\ u_{o2\mathrm{ref}}=0}. \tag{34}$$

In fact, considering that the dc side filter capacitor C_{dc} of the ac–dc converter is generally large, to some extent the ac system and dc system is decoupling, so the interaction between the two subsystem is limited [21].

Now, the specific T_2 can be given based on (31) and (34). Its expression is rewritten here

$$T_2 = (-Y'_{o1} + Y'_{i3} + Y'_{i4})^{-1} \tag{35}$$

and the stability of Bus 2 can be assessed through (35).

B. Bus 1

Similarly, when the stability of Bus 1 needs to be considered, for dc 1 and dc 2, there are

$$\begin{cases} i_{o1}(s) = Y_{ld1}(s)u_{o1}(s) = (Y'_{i3} + Y'_{i4})u_{o1}(s) \\ i_{o2}(s) = Y_{ld2}(s)u_{o2}(s) = \frac{1}{R_2}u_{o2}(s) \end{cases} \tag{36}$$

in which the sum of input admittance of dc 3 and dc 4 is the equivalent load of dc 1.

Substitute (36) into (20) and the input admittance of dc 1 Y'_{i1} and the input admittance DC 2 Y'_{i2} will be obtained. So the closed-loop transfer function of Bus 1 T_1 can be written as

$$T_1 = (Z'_{oac} + Y'_{i1} + Y'_{i2})^{-1}. \tag{37}$$

C. PCC

Finally, the input admittance of dc part has to be taken into account when the stability of PCC is discussed, where

$$Y_{i\mathrm{dc}} = Y'_1 + Y'_2 \tag{38}$$

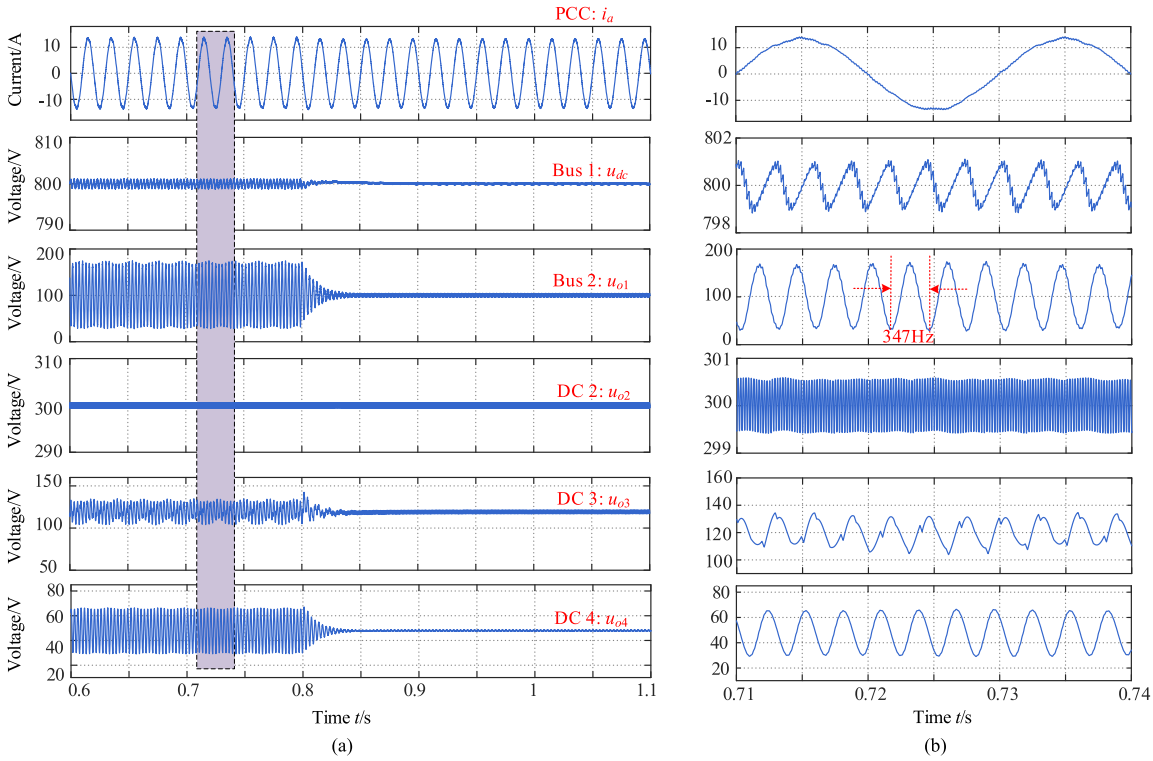

Fig. 11. Waveforms of PCC, buses, and converters. (a) Change the controller parameters k_{p1} and k_{i1} of DC 1 from 0.002 and 1.2 to 0.001 and 0.2 at 0.8 s and (b) is the local enlargement of (a).

substitute it into the small signal model of ac–dc converter and get the new input admittance Y'_{iac} of ac–dc converter, so the transfer function of PCC $\boldsymbol{T}_{ac}$ is

$$\boldsymbol{T}_{ac} = (\boldsymbol{Y}_g + \boldsymbol{Y}'_{iac})^{-1}. \tag{39}$$

After obtaining the transfer functions of each part, the eigenvalues of these transfer functions can be further solved and the system stability can be judged by analyzing these eigenvalues based on the stability assessment in Section III.

D. Stability Assessment for a Complex Cascaded System

When the number of cascades increases, theoretical modeling can be used to measure the effect of each converter, but at the cost of increasing the complexity of the model and the computer calculation time. It is also impractical to measure the impedance model of the two-terminal subsystem of a bus directly when the whole system is connected, because the system may not have a suitable steady-state operating point. Therefore, a gradual stability assessment strategy is proposed here. First, a system is divided into several subsystems based on the buses, and each subsystem contains some buses and converters. Second, the stability of each subsystem is ensured by the abovementioned modeling methods and criterion. Then, the impedance model of each subsystem is obtained by measurement and the stability of the whole system can be assessed based on the known connection relationships.

Furthermore, the advantage of using the above method is that the matrix dimension to be studied depends only on the number and type of the converters connected to the bus, so the dimension of each transfer function is not high, making it easy to calculate. However, due to the fact that the number of stability assessment is equal to the number of cascade buses, it may take more time to analyze the stability when the system's scale becomes large. A new admittance model is used in [29], [30], and [31], in which the input or output terminals of converters and passive networks are, respectively, transformed to Norton or Thevenin equivalent circuit, allowing the active equipment of the entire system to be integrated into a matrix for analysis. Although the model increases the dimension of the matrix, it greatly decreases the number of computation and stability assessment, making it more suitable for large-scale system. Hence, regarding future article, the new admittance model can be further combined with the PMD criterion to better determine the stability of the more complex ac/dc hybrid system with multiple buses.

V. Simulation Analysis

In order to verify the validity of the proposed stability assessment method for the multiple dc buses cascaded system, a simulation model based on Fig. 9(a) is built in MATLAB/Simulink. The detailed control structures can be seen in Figs. 3 and 7. Besides, the system parameters are listed in Table I.

First, when these converters are combined in the manner shown in Fig. 9(a), the transfer functions of dc buses and PCC can be obtained based on Sections II and IV. Then, the PMD criterion is used for stability analysis. The result can be seen in Fig. 10 and Table II. It shows that there exists a peak at about

TABLE I
PARAMETERS OF SYSTEM

Description		Value	Description		Value
Power grid	Grid voltage (rms)	U_g=220 V	Operating frequency		f_s=5 kHz
	Grid frequency	f_g=50 Hz			
AC–DC converter circuit parameters	Output voltage	U_{dc}=800 V	DC–DC converter circuit parameters	Output voltage	U_{o1}-U_{o4}/V 100,300,120,48
	Output capacitance	C_{dc}=4000 μF		Output power	P_1-P_4/kW 4, 2, 2, 2
	Filter inductance	L_{AC1}=1 mH, L_{AC1}=1 mH		Inductance	L_1-L_4/mH 2, 2, 2, 1
	Filter capacitance	C_f=40 μF		Capacitance	C_1-C_4/μF 400,400,600,300
AC–DC controller parameters	PLL	K_{p_PLL}=2, K_{i_PLL}=100	DC–DC controller parameters	DC 1	K_{p1}=2×10^{-3}, K_{i1}=1.2
	Voltage loop	K_{p_i}=1.2, K_{i_i}=100		DC 2	K_{p2}=2×10^{-3}, K_{i2}=1
	Current loop	K_{p_u}=1, K_{i_u}=20		DC 3	K_{p3}=1×10^{-3}, K_{i3}=0.2
				DC 4	K_{p4}=5×10^{-3}, K_{i4}=1

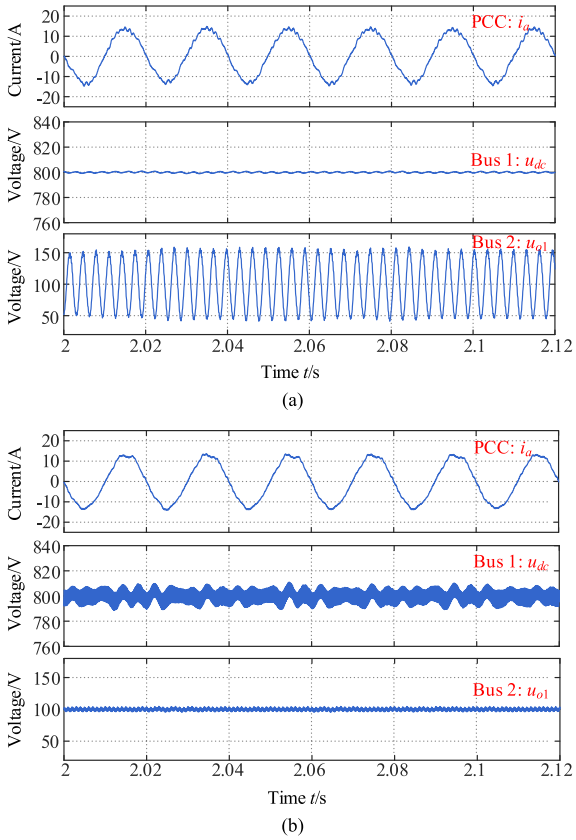

Fig. 12. Waveforms of PCC, Bus 1, and Bus 2 with different C_{dc}: (a) C_{dc} = 4000 μF and (b) C_{dc} = 100 μF.

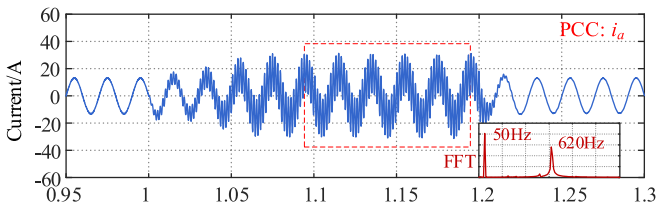

Fig. 13. Grid-connected current waveform when increasing L_g to 2.2 mH at 1 s and adjusting k_{p_i} from 1.2 to 0.5 at 1.2 s.

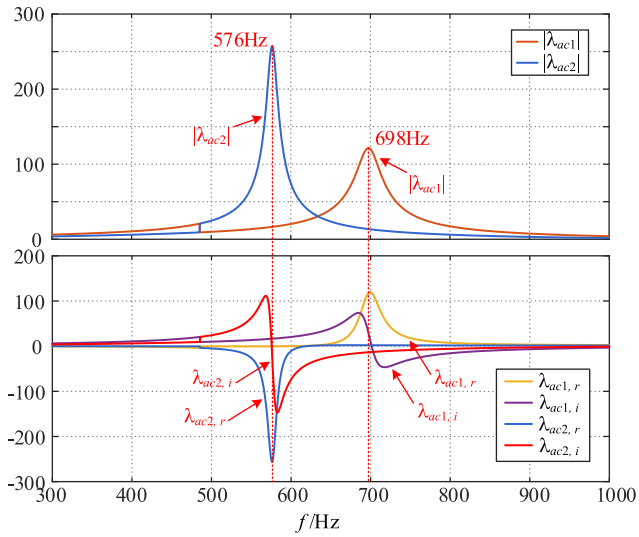

Fig. 14. Stability assessment of PCC when increasing L_g to 2.2 mH.

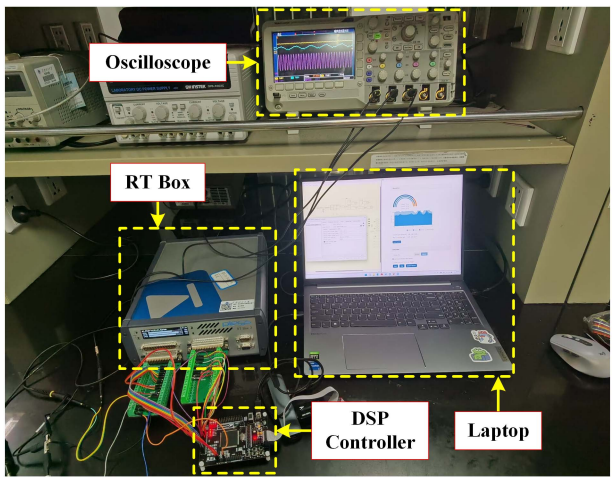

Fig. 15. Experiment platform.

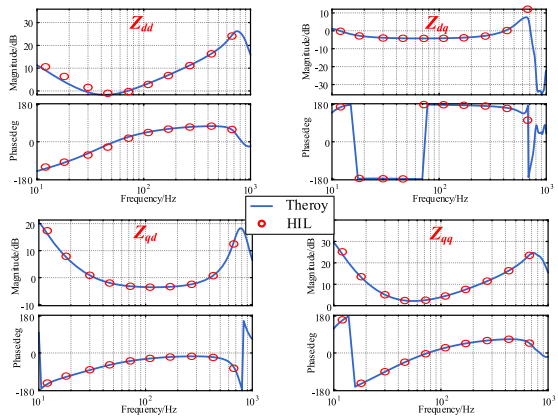

Fig. 16. Impedance bodes of $\boldsymbol{Z}_{\text{eq}} = \Delta \boldsymbol{u}_{dq} \Delta \boldsymbol{i}_{dq}^{-1}$.

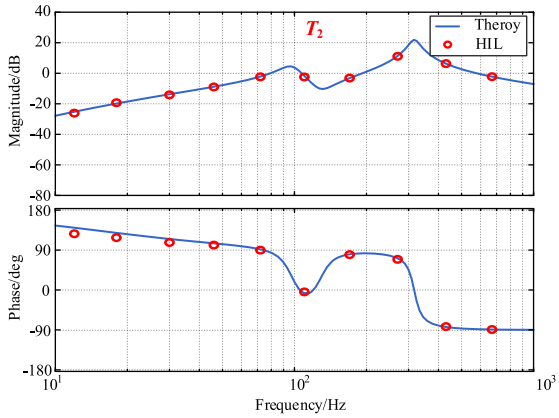

Fig. 17. Impedance bodes of T_2.

TABLE II
STABILITY ASSESSMENT OF PCC

	f/Hz	$T_{2,r}$	$k_{T2,i}$	$(T_{2,r} / k_{T2,i})$	Stability
T_2	348	<0	<0	>0	Unstable

348 Hz for the closed-loop transfer function of Bus 2 (i.e., T_2). Besides, the real part $T_{2,\ r}$ of T_2 and the slope of imaginary part $k_{T2,\ i}$ of T_2 are all less than 0, which indicate that Bus 2 is unstable. On the contrary, Bus 1 and PCC do not have the abovementioned characteristics and they are stable.

Furthermore, a simulation model is established in MATLAB/Simulink and its operating waveforms are shown in Fig. 11, in which i_a is the grid-connected current of A phase, u_{dc} is the output voltage of ac–dc converter and u_{oi} (i = 1, 2, 3, or 4) is the output voltage of dc i. It should be noted that these converters in the system are stable when each converter operates independently. And, it can be seen that the system becomes unstable after being connected according to Fig. 9(a). The main oscillation occurs in Bus 2 and its oscillation frequency is approximately 347 Hz, which is basically consistent with theoretical prediction. The voltage of Bus 1 and the current of PCC do not change much. Among these, the current at PCC

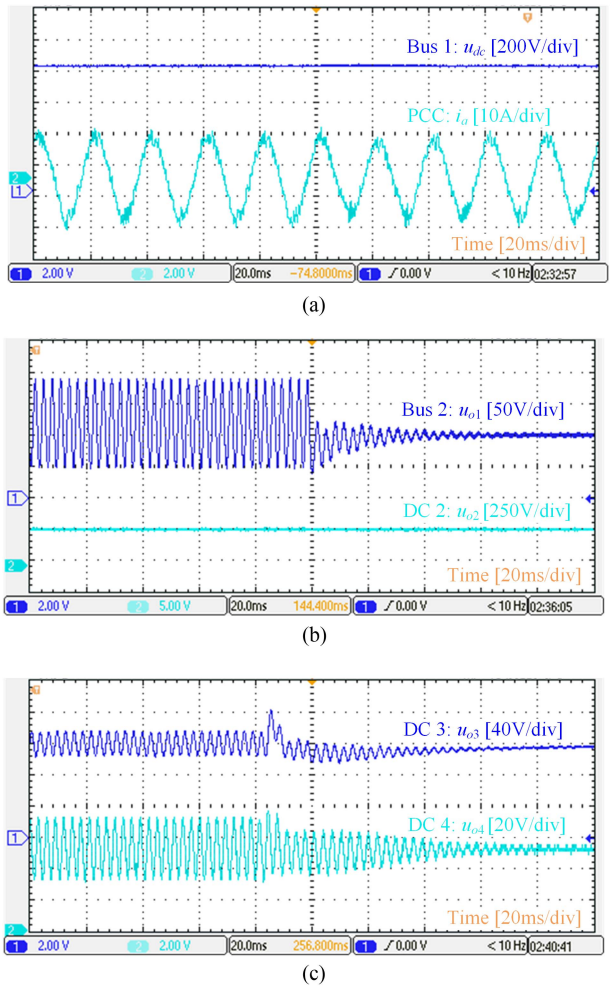

Fig. 18. Experiment waveforms.

(i.e., i_a) is almost undistorted, and the voltage ripple of Bus 1 (i.e., u_{dc}) is less than 0.5%. These are also consistent with previous analyses. In addition, the oscillations are transmitted to the outputs of dc 3 and dc 4, as shown in Fig. 11, indicating that in a cascaded system these levels are coupled to each other and a local instability may affect the stability of other parts. To restore stability to the system, attempt to adjust the parameter of dc 1, which is directly connected to the Bus 2. As seen in Fig. 11, the system returns to stable after the controller parameters k_{p1} and k_{i1} of dc 1 are adjusted from 0.002 and 1.2 to 0.001 and 0.2 at 0.8 s.

As mentioned in Section IV, a filter capacitor with large enough capacitance can weaken the mutual fluence between the ac–dc converter and the dc–dc converters. It seems that the larger the capacitance value, the more stable the system. For that, the effect of capacitor of Bus 1 is taken as an example to be investigated and Fig. 12 gives several waveforms of the system under two different values of C_{dc}.

Although the oscillation of Bus 1 and PCC becomes slightly more severe when C_{dc} decreases from 4000 to 100 μF, it can also be found that the oscillation amplitude of Bus 2 is greatly reduced. The peaks of the closed-loop transfer function's

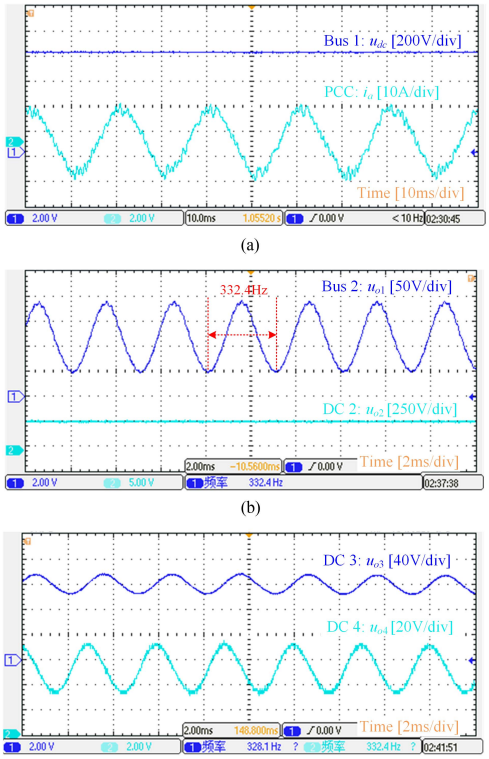

Fig. 19. Local enlargement of Fig. 18.

TABLE III
PEAKS OF CLOSED-LOOP TRANSFER FUNCTIONS OF BUSES

	4000 μF	100 μF
Bus 2($\lvert T_2\rvert$)	41.9	17.6
Bus 1($\lvert T_1\rvert$)	0.13	5.50
PCC($\lvert\lambda_{ac}\rvert$)	3×10^{-3}	5×10^{-3}

amplitudes are listed in Table III. It shows that for Bus 2, $|T_2|$ jumped from 41.9 to 17.6 and the peak of Bus 1 and PCC have a certain rise. That is consistent with the simulation. Based on above results, it can be found that a larger capacitor can reduce the degree to which oscillations propagate from one part of the system to other parts. And in this example, the coupling between the ac–dc converter and the dc–dc converter is cut down. However, the interaction caused by a smaller capacitor might make the whole system buses more stable. It means that sometimes a certain coupling between the converters can be beneficial for reducing the oscillation of the overall system buses. Its mechanism and how to evaluate this effect with a more appropriate indicator could be our future article.

Finally, the stability issue caused by the grid impedance is analyzed. Increase L_g to 2.2 mH at 1 s and the ac–dc converter also oscillates obviously. Then, tune the current loop parameter $k_{p\cdot i}$ from 1.2 to 0.5 at 1.2 s and the system becomes stable again. Its waveforms are shown in Fig. 13 and its stability assessment can be seen in Fig. 14 and Table IV. It can be found from Fig. 13 that the system loses stability at 620 Hz.

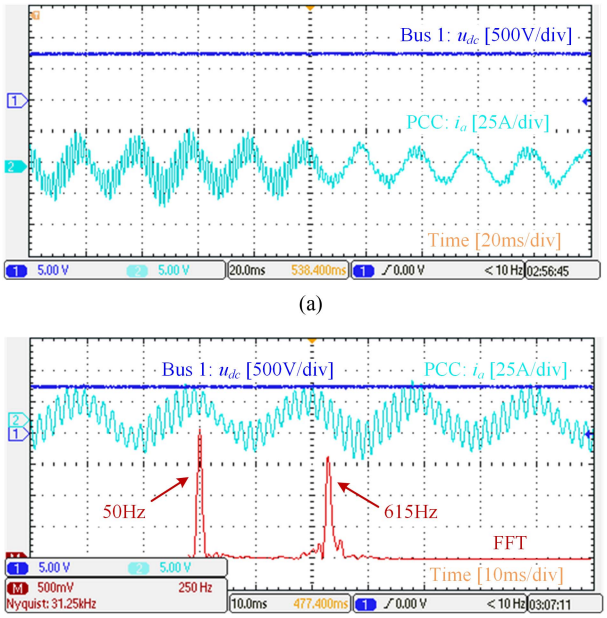

Fig. 20. (a) Experiment waveforms of i_a and $u_{\rm dc}$ when L_g is set as 2.2 mH and (b) is the local enlargement of (a).

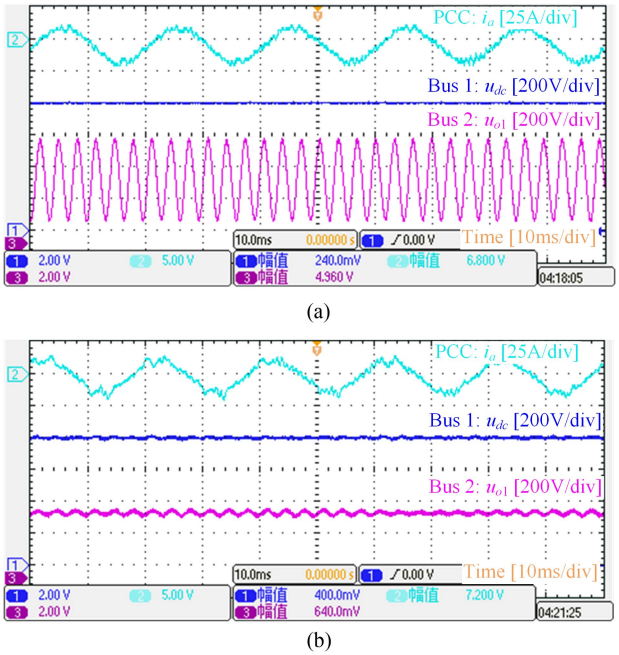

Fig. 21. Experiment waveforms of PCC, Bus 1, and Bus 2 with different $C_{\rm dc}$: (a) $C_{\rm dc}=4000$ μF and (b) $C_{\rm dc}=100$ μF.

TABLE IV
STABILITY ASSESSMENT OF PCC

	f/Hz	$\lambda_{ac,r}$	$k_{\lambda ac,i}$	($\lambda_{ac,r}$/ $k_{\lambda ac,i}$)	Stability
λ_{ac1}	698	>0	<0	<0	Stable
λ_{ac2}	576	<0	<0	>0	Unstable

On the other hand, Fig. 14 shows that the frequency of the main harmonic component is about 576 Hz. The difference between the simulation and the stability assessment is that the former is in *abc* coordinate and the latter is in *dq* coordinate, there is a difference of 50 Hz between them. So it indicated that the simulation result is basically in accordance with the theoretical predictions.

VI. Experiment Verification

To further validate the effectiveness of the proposed method and analyses, a hardware-in-loop test platform was built based on the circuit topology and control structure introduced in Section II [see Figs. 3, 7, and 9(a) for details], as shown in Fig. 15. The main circuit of the platform is simulated by Plexim's RT Box, and the controller algorithms are implemented in the hardware of a TMS320F28335 digital signal processor (DSP). Specifically, the circuit model is constructed by the electrical components in the upper computer software, and then translated into the RT box, while several I/O boards are used to transmit electrical and control signals between DSP and RT Box.

First, the impedance model of PCC and Bus 2 are obtained through sweeping frequency test (i.e., $\boldsymbol{Z}_{\text{eq}} = \Delta \boldsymbol{u}_{dq} \Delta \boldsymbol{i}_{dq}^{-1}$ and T_2, respectively), and Figs. 16 and 17 give the detailed comparison of the results from the theory model (introduced in Section II) and the measuring model, which are in agreement with each other.

When the parameters are in accordance with Table I, the detailed waveforms of the system are shown in Fig. 18 and its local enlargements are given in Fig. 19. Besides, when the grid impedance L_g is set as 2.2 mH, the experiment results are shown in Fig. 20. They can be seen that the system becomes unstable and the resonance frequency of Bus 2 and PCC are approximately 332.4 and 615 Hz, respectively. The error between experiment and theory analysis is within 5%. Furthermore, change corresponding controller parameters and the system returns to normal operation.

Other than these, decrease C_{dc} from 4000 to 100 μF and the waveforms of three buses are shown in Fig. 21. The results indicated that a smaller capacitor might weaken the oscillation of the whole system in some cases. It can be hard to evaluate the effect of circuit parameter on the stability, especially for the complex system studied in this article, containing different kind of converters and many buses. However, it also provides many possibilities to improve the system stability and will be further investigated.

VII. Conclusion

In this article, the stability of a cascaded system with multiple dc buses is discussed. On the one hand, the mathematical model of the system is derived in detail and the mutual influence between various levels of buses and converters is taken into account. On the other hand, a cascaded system stability assessment method based on the PMD criterion is proposed and a further stability analysis procedure suitable for the complex cascaded system is given. Compared with the traditional NC, the proposed method has simple steps and does not need to consider the possible RHP poles in the open-loop transfer function. Besides, the instability frequency of the system can be predicted. In addition, the effect of dc bus capacitor is explored and the result shows that increasing the coupling between the converters appropriately may reduce the oscillation of the overall system buses. It provides new possibility for the cascaded system controllers design and will be further investigated in the future. Furthermore, a cascaded system with two dc buses and several kinds of converters are designed in this article, and the effectiveness of the proposed method is verified by simulation and experiment.

Appendix

The detailed transfer function expressions in Section II

$$\begin{cases} \boldsymbol{Z}_{LAC1} = \begin{bmatrix} sL_{AC1} & -\omega_0 L_{AC1} \\ \omega_0 L_{AC1} & sL_{AC1} \end{bmatrix}, \ \boldsymbol{Z}_{LAC2} = \begin{bmatrix} sL_{AC2} & -\omega_0 L_{AC2} \\ \omega_0 L_{AC2} & sL_{AC2} \end{bmatrix} \\ \boldsymbol{Y}_{Cf} = \begin{bmatrix} sC_f & -\omega_0 C_f \\ \omega_0 C_f & sC_f \end{bmatrix} \end{cases} \tag{40}$$

$$G_{\text{PI\_PLL}}(s) = K_{p\_\text{PLL}} + \frac{K_{i\_\text{PLL}}}{s} \tag{41}$$

where $G_{\text{PI·PLL}}$ is the PI controller of PLL

$$\begin{cases} \boldsymbol{G}_{iu\text{dc}} = -\frac{3}{4sC_{\text{dc}}} \left(\frac{2}{U_{\text{dc}}} \begin{bmatrix} I_d & I_q \\ 0 & 0 \end{bmatrix} \boldsymbol{G}_2^{-1} + \begin{bmatrix} D_d & D_q \\ 0 & 0 \end{bmatrix} \boldsymbol{G}_3 \right) \\ \boldsymbol{G}_{u\text{udc}} = -\frac{3}{4sC_{\text{dc}}} \left(-\frac{2}{U_{\text{dc}}} \begin{bmatrix} I_d & I_q \\ 0 & 0 \end{bmatrix} \boldsymbol{G}_2^{-1} \boldsymbol{G}_1 + \begin{bmatrix} D_d & D_q \\ 0 & 0 \end{bmatrix} \boldsymbol{G}_4 \right). \end{cases} \tag{42}$$

Buck:

$$G_{\text{Buck}} = \frac{1}{1 + s^2 LC} \tag{43}$$

$$\begin{cases} Y_i = G_{\text{Buck}}[sD^2 C + \frac{D^2}{sL}], \quad Y_{oi} = -\frac{D}{sL} \\ G_{dii} = G_{\text{Buck}} \left[s^2 LCI_o + sCDU_i + I_o + \frac{DU_i}{sL} \right] \\ Y_{io} = \frac{D}{sL}, \quad Y_o = \frac{1}{G_{\text{Buck}}(sL)} \\ G_{dio} = \frac{U_i}{sL}. \end{cases} \tag{44}$$

Boost:

$$G_{\text{Boost}} = \frac{1}{s^2 LC + (1-D)^2} \tag{45}$$

$$\begin{cases} Y_i = G_{\text{Boost}} \left[(sC) + \frac{(1-D)^2}{sL} \right], \quad Y_{oi} = -\frac{1-D}{sL} \\ G_{dii} = \frac{G_{\text{Boost}} \left[-s(1-D)LI_i + (1-D)^2 U_o \right]}{sL} \\ Y_{io} = \frac{1-D}{sL}, \quad Y_o = \frac{1}{G_{\text{Boost}}(sL)} \\ G_{dio} = \frac{-sLI_i + (1-D)U_o}{sL}. \end{cases} \tag{46}$$

References

[1] L. Xiong, X. Liu, Y. Liu, and F. Zhuo, "Modeling and stability issues of voltage-source converter-dominated power systems: A review," *CSEE J. Power Energy Syst.*, vol. 8, no. 6, pp. 1530–1549, Nov. 2022.

[2] M. Li, X. Zhang, Z. Guo, J. Wang, and F. Li, "The dual-mode combined control strategy for centralized photovoltaic grid-connected inverters based on double-split transformers," *IEEE Trans. Ind. Electron.*, vol. 68, no. 12, pp. 12322–12330, Dec. 2021.

[3] X. Wang, K. Qin, X. Ruan, D. Pan, Y. He, and F. Liu, "A robust grid-voltage feedforward scheme to improve adaptability of grid-connected inverter to weak grid condition," *IEEE Trans. Power Electron.*, vol. 36, no. 2, pp. 2384–2395, Feb. 2021.
[4] B. Liu, H. Ben, X. Zhang, T. Meng, and X. Wang, "Stabilization of a cascaded AC–DC–DC system with small bus capacitance based on small signal analysis," *IEEE Trans. Ind. Appl.*, vol. 54, no. 5, pp. 4650–4659, Sep./Oct. 2018.
[5] H. Cai, J. Xiang, and W. Wei, "Modelling, analysis and control design of a two-stage photovoltaic generation system," *IET Renewable Power Gener.*, vol. 10, pp. 1195–1203, 2016.
[6] Z. Li and M. Shahidehpour, "Small-signal modeling and stability analysis of hybrid AC/DC microgrids," *IEEE Trans. Smart Grid*, vol. 10, no. 2, pp. 2080–2095, Mar. 2019.
[7] P. T. Krein, J. Bentsman, R. M. Bass, and B. L. Lesieutre, "On the use of averaging for the analysis of power electronic systems," *IEEE Trans. Power Electron.*, vol. 5, no. 2, pp. 182–190, Apr. 1990.
[8] M. Rasheduzzaman, J. A. Mueller, and J. W. Kimball, "An accurate small-signal model of inverter-dominated islanded microgrids using (DQ) reference frame," *IEEE J. Emerg. Sel. Top. Power Electron.*, vol. 2, no. 4, pp. 1070–1080, Dec. 2014.
[9] M. Su, Z. Liu, Y. Sun, H. Han, and X. Hou, "Stability analysis and stabilization methods of DC microgrid with multiple parallel-connected DC–DC converters loaded by CPLs," *IEEE Trans. Smart Grid*, vol. 9, no. 1, pp. 132–142, Jan. 2018.
[10] M. Cespedes and S. Jian, "Impedance modeling and analysis of grid-connected voltage-source converters," *IEEE Trans. Power Electron.*, vol. 29, no. 3, pp. 1254–1261, Mar. 2014.
[11] B. Wen, D. Boroyevich, R. Burgos, P. Mattavelli, and Z. Shen, "Analysis of D-Q small-signal impedance of grid-tied inverters," *IEEE Trans. Power Electron.*, vol. 31, no. 1, pp. 675–687, Jan. 2016.
[12] Y. Liao, X. Wang, and X. Wang, "Frequency-domain participation analysis for electronic power systems," *IEEE Trans. Power Electron.*, vol. 37, no. 3, pp. 2531–2537, Mar. 2022.
[13] W. Rui, S. Qiuye, M. Dazhong, and H. Xuguang, "Line impedance cooperative stability region identification method for grid-tied inverters under weak grids," *IEEE Trans. Smart Grid*, vol. 11, no. 4, pp. 2856–2866, Jul. 2020.
[14] D. Lu, X. Wang, and F. Blaabjerg, "Impedance-based analysis of DC-link voltage dynamics in voltage-source converters," *IEEE Trans. Power Electron.*, vol. 34, no. 4, pp. 3973–3985, Apr. 2019.
[15] M. Li et al., "The control strategy for the grid-connected inverter through impedance reshaping in *q*-axis and its stability analysis under a weak grid," *IEEE Trans. Emerg. Sel. Topics Power Electron.*, vol. 9, no. 3, pp. 3229–3242, Jun. 2021.
[16] J. Guo et al., "Impedance analysis and stabilization of virtual synchronous generators with different DC-link voltage controllers under weak grid," *IEEE Trans. Power Electron.*, vol. 36, no. 10, pp. 11397–11408, Oct. 2021.
[17] Z. Zou et al., "Modeling and control of a two-bus system with grid-forming and grid-following converters," *IEEE J. Emerg. Sel. Topics Circuits Syst.*, vol. 10, no. 6, pp. 7133–7149, Dec. 2022.
[18] Y. Zhang, X. Yuan, and X. Wu, "A novel decoupling control approach for improving dynamic performance and stability of multiple grid-connected converters," *IEEE Trans. Ind. Electron.*, vol. 69, no. 9, pp. 8613–8624, Sep. 2022.
[19] X. Wang, F. Blaabjerg, and P. C. Loh, "An impedance-based stability analysis method for paralleled voltage source converters," in *Proc. IEEE Int. Power Electron. Conf.*, 2014, pp. 1529–1535.
[20] M. Lu, X. Wang, P. C. Loh, and F. Blaabjerg, "Resonance interaction of multiparallel grid-connected inverters with LCL filter," *IEEE Trans. Power Electron.*, vol. 32, no. 2, pp. 894–899, Feb. 2017.
[21] Y. Li, Z. Shuai, J. Fang, X. Wu, and Z. J. Shen, "Small-signal stability analysis method for hybrid AC–DC systems with multiple DC buses," *IEEE J. Emerg. Sel. Topics Circuits Syst.*, vol. 11, no. 1, pp. 17–27, Mar. 2021.
[22] J. Siegers, S. Arrua, and E. Santi, "Stabilizing controller design for multi-bus MVdc distribution systems using a passivity-based stability criterion and positive feedforward control," *IEEE J. Emerg. Sel. Topics Power Electron.*, vol. 5, no. 1, pp. 14–27, Mar. 2017.
[23] L. Orellana, L. Sainz, E. Prieto-Araujo, and O. Gomis-Bellmunt, "Stability assessment for multi-infeed grid-connected VSCs modeled in the admittance matrix form," *IEEE Trans. Circuits Syst. I: Reg. Papers.*, vol. 68, no. 9, pp. 3758–3771, Sep. 2021.
[24] L. Orellana, L. Sainz, E. Prieto-Araujo, M. Cheah-Mané, H. Mehrjerdi, and O. Gomis-Bellmunt, "Study of black-box models and participation factors for the positive-mode damping stability criterion," *Int. J. Elect. Power Energy Syst.*, vol. 148, Jan. 2023, Art. no. 10857.
[25] J. Ma, L. Wang, and P. Cheng, "Research on the mechanism of simultaneous instability of *dq* frame sub- and super-synchronous oscillations in grid-tied converter," *IEEE Trans. Power Syst.*, vol. 38, no. 3, pp. 2895–2913, May 2023.
[26] A. G. J. Macfarlane and I. Postlethwaite, "The generalized Nyquist stability criterion and multivariable root loci," *Int. J. Control*, vol. 25, no. 1, pp. 81–127, Jan. 1977.
[27] H. Liu, X. Xie, and W. Liu, "An oscillatory stability criterion based on the unified *dq*-frame impedance network model for power systems with high-penetration renewables," *IEEE Trans. Power Syst.*, vol. 33, no. 3, pp. 3472–3485, May 2018.
[28] F. Cecati, R. Zhu, S. Pugliese, M. Liserre, and X. Wang, "State feedback reshaping control of voltage source converter," *IEEE Trans. Power Electron.*, vol. 37, no. 12, pp. 14280–14293, Dec. 2022.
[29] J. Pedra, L. Sainz, and L. Monjo, "Three-port small signal admittance-based model of VSCs for studies of multi-terminal HVDC hybrid AC/DC transmission grids," *IEEE Trans. Power Syst.*, vol. 36, no. 1, pp. 732–743, Jan. 2021.
[30] H. Zhang, M. Mehrabankhomartash, M. Saeedifard, Y. Zou, Y. Meng, and X. Wang, "Impedance analysis and stabilization of point-to-point HVDC systems based on a hybrid AC–DC Impedance model," *IEEE Trans. Ind. Electron.*, vol. 68, no. 4, pp. 3224–3238, Apr. 2021.
[31] Y. Zhang, D. Duckwitz, N. Wiese, and M. Braun, "Extended nodal admittance matrix based stability analysis of HVDC connected AC grids," *IEEE Access*, vol. 10, pp. 55200–55212, 2022.

Yuhang Yang (Student Member, IEEE) received the B.S. degree in electrical engineering from the Fuzhou University, Fuzhou, China, in 2021. He is currently working toward the master's degree in electrical engineering with the South China University of Technology, Guangzhou, China.

His research interests include the study of modeling and stability analysis of grid-connected converter and system.

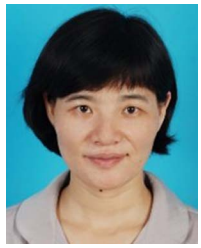

Yanfeng Chen (Member, IEEE) received the M.S. degree in power electronics technology from the Wuhan University, Wuhan, China, in 1995, and the Ph.D. degree in circuits and systems from the South China University of Technology, Guangzhou, China, in 2000.

From 2005 to 2006, she was a Research Associate with the Department of Electronic and Information Engineering, Hong Kong Polytechnic University, Hong Kong. She is currently a Professor with the School of Electric Power, South China University of Technology. She has authored or coauthored three books, and more than 50 papers and 50 patents. Her research interests include modeling and analysis of nonlinear systems and power electronics.

Bo Zhang (Fellow, IEEE) was born in Shanghai, China, in 1962. He received the B.S. degree in electrical engineering from the Zhejiang University, Hangzhou, China, in 1982, the M.S. degree in power electronics from the Southwest Jiaotong University, Chengdu, China, in 1988, and the Ph.D. degree in power electronics from the Nanjing University of Aeronautics and Astronautics, Nanjing, China, in 1994.

He is currently a Professor with the School of Electric Power, South China University of Technology, Guangzhou, China. He has authored or coauthored more than 600 papers and held more than 170 patents. He has authored nine monographs. His research interests include nonlinear analysis and control of power electronics, wireless power transfer technology, and ac drives.

Dongyuan Qiu (Senior Member, IEEE) was born in China, in 1972. She received the B.Sc. and M.Sc. degrees in automation from the South China University of Technology, Guangzhou, China, in 1994 and 1997, respectively, and the Ph.D. degree in electronic engineering from the City University of Hong Kong, Hong Kong, in 2002.

She is currently a Professor with the School of Electric Power, South China University of Technology. She has authored or coauthored three books and more than 200 papers and holds about 100 patents. Her research interests include modeling of power electronic converters, wireless power transfer, and fault diagnosis.

Dr. Qiu is an Associate Editor for IEEE TRANSACTIONS ON POWER ELECTRONICS.

Fan Xie (Member, IEEE) received the B.S. and M.S. degrees in physics and physical electronics from the School of Physics and Electron Engineering, Guangzhou University, Guangzhou, China, in 2008 and 2011, respectively, and the Ph.D. degree in power electronics from the South China University of Technology, Guangzhou, China, in 2014.

In 2014, he joined the School of Electric Power, South China University of Technology, where he has been an Associate Professor, since 2018. His research interests include nonlinear dynamics of power electronic circuits and control of power supplies and ac drives.